Proceedings of 20th International Congress on Acoustics, ICA 2010

23-27 August 2010, Sydney, Australia

Aperture Synthesis on 2-D Ultrasonic Transducer Arrays for Projection Imaging of Biological Media

Krzysztof J. Opieliński, Tadeusz Gudra

Institute of Telecommunications, Teleinformatics and Acoustics, Wroclaw University of Technology, Wybrzeze Wyspianskiego 27, 50-370 Wroclaw, Poland

PACS: 43.60.Fg; 43.38.Hz; 43.80.Ev

ABSTRACT

This paper offers several schemes of activating a small number of elements in a pair of 2-D transmitting and receiving plane arrays for imaging of the structure of biological media by means of the ultrasonic projection (transmission method). Such aperture synthesis with adequately switched small subarrays (with accordance to the scanning method) allows achieving a significant directivity and the increased ultrasonic wave intensity with an acceptable input electrical impedance decrease. The novel approach in this work is reflected in wave beam profile modelling based on a simple simulation of the spatial distribution of the results of multiplying the transmitted and received ultrasonic wave field as a product of an effective transmitting-receiving aperture, rather than the coarray, the aperture or the point spread function (PSF) used in the echo method. In the end a simulation algorithm was developed and presented and the calculations and measurements of ultrasonic wave field distributions for some essential aperture configurations were compared.

INTRODUCTION

A number of authors working in the field of medical imaging have recently suggested the use of multielement arrays and investigated methods of selecting the optimal number and distribution of the elements of transmitting and receiving apertures [1,2,3,4,5,6,7,8,9,10,11,12,13]. It is also one of many methods that suppress grating side lobes (caused by aliasing effect) [1,4,6,8,10,14] and hence it allows to relax the criterion of the maintaining a suitably small distance (pitch) between the centres of adjacent transducers (less than a half wave length) in the 2-D array, which itself is a difficult requirement to realise in practice [1,2,4,6,7,10,14].

The majority of the 2-D ultrasonic multielement arrays are designed for miniature 3-D volumetric medical endoscopic imaging, where they serve as intracavital probes providing unique opportunities for guiding surgeries or minimally invasive therapeutic procedures [8,9,10,15]. Most of them are intended for operation using echo method [6]. Aperture synthesis of a 2-D sending and receiving ultrasonic transducer array, presented in this work, is used to improve projection imaging of biological media [16,17,18,19,20,21,22]. Ultrasonic projection imaging (the transmission method) uses information from ultrasonic pulses propagating through an object's structure in order to produce qualitative images showing an orthogonal projection of the studied structure in the form of distribution of average values of the measured acoustic parameter for one or more surfaces perpendicular to the direction of incidence of ultrasonic waves (similarly to roentgenography) [19,20,21,22,23]. It is additionally possible to simultaneously image a few acoustic parameters, which are digitally determined on the basis of information obtained directly from ultrasonic pulses propagating through a structure (e.g. amplitude, runtime, mid frequency down shift). This allows simultaneous generation of a few different projection images each of which represents a different feature of the structure [20,21,23]. Such complex characteristics can be of significant importance in e.g. the process of diagnosing cancerous changes in tissue. If a pair of 2-D ultrasonic transducer arrays (sending and receiving one) with fast electronic switching of single elementary transducers or transducer subarrays is used, it is possible to acquire images in pseudo-real time (with constant delay for data buffering and processing) [16,17,18,19,22]. Additionally, rotation of a pair of 2-D sending and receiving ultrasonic transducer arrays means it is possible to acquire projection images from a sufficient range of directions around the studied object, which in turn allows tomographic reconstruction of a 3-D quantitative image of the internal structure of an object in parallel-ray projection geometry [23]. It can serve as an alternative to divergent geometry (multielement ultrasonic ring probe [24,25,26]). The quality of a projection image and the precision of structure reconstruction in a projection predominantly depend on the signal/noise ratio in the receiving setup, the number and sizes of elementary ultrasonic transducers of the sending and receiving array and the pitch between them. Smaller elementary transducers mean lower level of acoustic pressure generated in a studied medium. This, in turn, causes lower signal/noise ratio in the receiving setup. Decreasing the pitch between the transducers of the array to less than half of the wave length is difficult as it is necessary to attach electrodes. Bigger pitches result in occurrence of grating side lobes, which cause imaging errors. There is, however, an excellent way to achieve high amplitude of the received signal in a transmission system of a 2-D sending and receiving ultrasonic transducer array. It can be done by means of suitable synthesis of scanning aperture of those transducers, which

will additionally guarantee high directivity and reduction of the occurrence of grating side lobes (apodization).

SYNTHESIS OF SCANNING APERTURE OF ARRAYS

Wave beam profile modelling

The easiest method of scanning a medium by means of ultrasonic projection is activating opposite pairs of elementary transducers of a sending and receiving array in a one to one configuration (Figure 1).

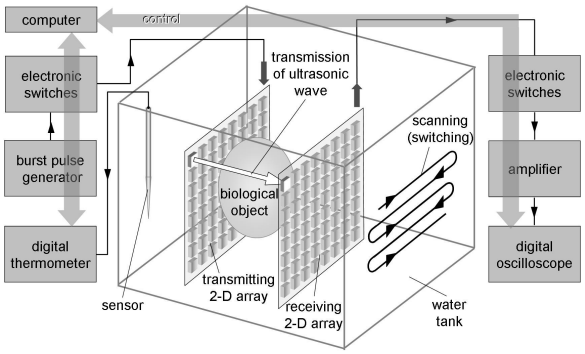

Figure 1. A block diagram of ultrasonic projection imaging.

Wave beam profile modelling, which ensures increase of the wave intensity and directivity, can be realised by switching suitable pairs of array transducer subarrays (Figure 2) with a step of one transducer [1,4,6,7,8,9,10].

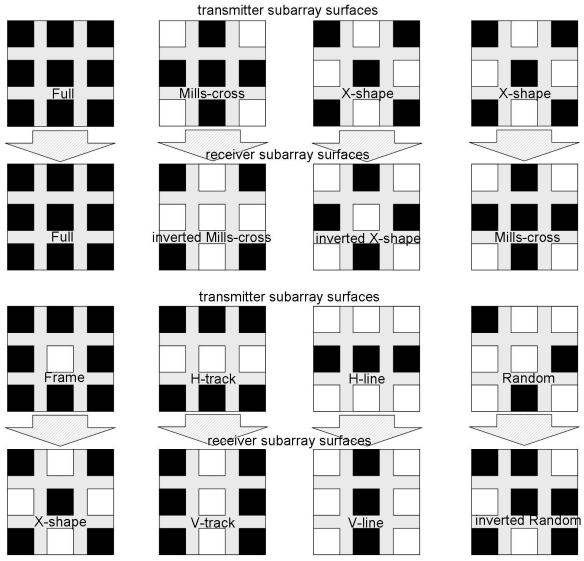

Figure 2. Selected combinations of sending-receiving apertures in a transmission scanning system of 3 x 3 transducers.

The scanning setup size (subarray N_s x N_s transducers, where N_s is usually an odd number) should not be too big because it limits the area of the scanned surface by $(N_s - 1)\cdot d$ horizontally and vertically, where d indicates the distance between the centres of transducers. Additionally, the larger the subarrays, the more side lobes occur. It is also necessary to consider the input electrical impedance of the subarray, which decreases with higher number of simultaneously activated parallelly connected transducers. In order to achieve maximum transduction efficiency, piezoceramic ultrasonic transducers of projection arrays are usually activated by means of narrow-band burst type pulses (from several to slightly over a dozen cycles of sine wave signal) produced by low power voltage generators with output impedance of about 50 Ω. If input impedance of the subarray connected to the generator is close to 50 Ω, the pulse voltage drops, which causes decrease of intensity of the generated ultrasonic wave. Moreover, electronic switches used to turn the array transducers on and off have non-zero, finite impedance, which affects attenuation of the propagated sent and received signals, especially if the impedance of the transducers is small. A setup of electronic switches and connection cables can also significantly change the input capacitance of transducers [13].

Method of calculation of acoustic field distribution

In order to synthesize, model and optimize scanning aperture of 2-D projection arrays it is necessary to be able to visualise ultrasonic wave beam profile in a sending-receiving setup to check directivity and the number and level of side lobes occurrence. The ultrasonic echo method uses the coarray, the aperture or the point spread function (PSF) for that purpose [5,8,9,27]. The novel approach in our work is reflected in wave beam profile modelling based on a simple simulation of the spatial distribution [13,24,25] of the results of multiplying the transmitted and received ultrasonic wave field as a product of an effective transmitting-receiving aperture. In order to calculate 3-D distribution of acoustic field generated in a medium by a 2-D ultrasonic array, consisting of evenly arranged square piezoceramic transducers, the authors developed an easy and effective method of numerical sum of fields of the elementary transducers [13] by means of the following formula:

$$p = \left| \sum_{n=0}^{N-1} \sum_{m=0}^{M-1} -j \frac{\rho c k a^2}{2\pi R(m,n)} \cdot V_o(m,n) \cdot A_\theta \cdot B_\varphi \cdot e^{j(\omega t - kR(m,n))} \right|, \quad (1)$$

where

$$A_\theta = \frac{\sin\left(\frac{ka\sin(\theta(n))}{2}\right)}{\frac{ka\sin(\theta(n))}{2}}, \quad (2)$$

$$B_\varphi = \frac{\sin\left(\frac{ka\sin(\varphi(m,n))}{2}\right)}{\frac{ka\sin(\varphi(m,n))}{2}}, \quad (3)$$

where: p – acoustic pressure, ρ – medium density, c – sound velocity in the medium, k – wave number, a – transducer side length, M – number of array rows, N – number of array columns, $R(m,n)$, $\theta(m,n)$, $\varphi(m,n)$ – polar coordinates of the distribution point modified in relation to the position of the transducer in the array, $V_o(m,n)$ – acoustic velocity for an array transducer. Value of acoustic pressure $p(x,y,z)$ for all active elements of the array is calculated as a sum of pressure values p_{mn} for a single element in many points of the medium with specified acoustic velocity values $V_o(m,n)$. If the attitude of the array in Cartesian coordinate system is such, that the x coordinate indicates the direction along the width of the array, the y coordinate indicates the direction along the height of the array and the z coordinate indicates the distance from the surface of the array along its axis (Figure 3), the following equations are valid:

$$r(n) = \sqrt{x(n)^2 + z^2}, \quad (4)$$

$$R(m,n) = \sqrt{r(n)^2 + y(m)^2} = \sqrt{x(n)^2 + y(m)^2 + z^2}, \quad (5)$$

$$\sin\theta(n) = \frac{x(n)}{r(n)} = \frac{x(n)}{\sqrt{x(n)^2 + z^2}}, \tag{6}$$

$$\sin\varphi(m,n) = \frac{y(m)}{R(m,n)} = \frac{y(m)}{\sqrt{x(n)^2 + y(m)^2 + z^2}}. \tag{7}$$

If array transducers are marked as shown in Figure 3, it is possible for the number of array rows $m = 0, 1, 2, \ldots, M-1$ and the number of array columns $n = 0, 1, 2, \ldots, N-1$, to define modified coordinates $x(n)$ and $y(n)$ as follows:

$$x(n) = x + (N - 1 - 2\cdot n)\cdot\frac{d}{2}, \tag{8}$$

$$y(m) = y + (M - 1 - 2\cdot m)\cdot\frac{d}{2}. \tag{9}$$

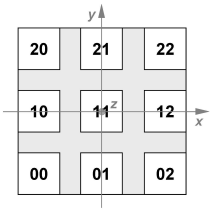

Figure 3. The method of marking and locating the transducers of the array.

The developed method of calculating 3-D distribution of acoustic field generated by a 2-D ultrasonic array allows detailed visualisation of the shape of wave beam in any plane in relation to the array, although acoustic velocity $V_o(m,n)$, which is in direct proportion to the amplitude of the voltage $U(m,n)$ powering the elementary transducer makes it possible to simulate acoustic field distribution when the array transducers are not activated in a regular fashion (e.g. as a result of diversified electromechanical parameters, array construction flaws, the effect of electrical parameters of switches, switch and transducer crosstalks) [12,13,28]. The effectiveness of a transmitting transducer can be estimated using a piezoelectric coefficient d_{ik} [m/V] of piezoceramic material:

$$d_{ik} = \frac{\Delta g}{U}, \tag{10}$$

which determines the relation between the maximum increase of the thickness Δg of a plate vibrating in thickness resonance f_r and voltage amplitude (peak) U. Acoustic velocity of the vibration of a plate surface can be determined based on the following formula:

$$V_o = 4\cdot\Delta g\cdot f_r. \tag{11}$$

Using the developed formula (1) with the time diversification $t \rightarrow t(m,n)$ it is also possible to simulate delays in activation of the array transducers in order to focus or steer the wave beam.

Formula (1) was used to calculate distribution of acoustic field generated in water by square transducer apertures (shown in Figure 2) in a 3 x 3 subarray. It was assumed that there are no delays of signals in the subarray and that all the transducers share the same acoustic velocity. Parameter values used for the calculations are shown in Table 1.

Figure 4 shows acoustic field distributions $p(x,y,z)$ in greyscale (from black to white) calculated in plane $x = y = -25$ mm ÷ 25 mm, at the distance $z_o = 50$ mm from the surface of the subarray, with resolution of $\Delta x = \Delta y = 0.5$ mm for selected apertures.

Table 1. Parameter values used for the calculations.

N_s	a [mm]	d [mm]	f [MHz]	ρ [kg/m^3]	c [m/s]	V_o [m/s]
3	1.6	2.5	2	1000	1490	0.1

Figure 5 compares the distribution of the values of the calculated acoustic pressure for the line of $y = 0$ images from Figure 4.

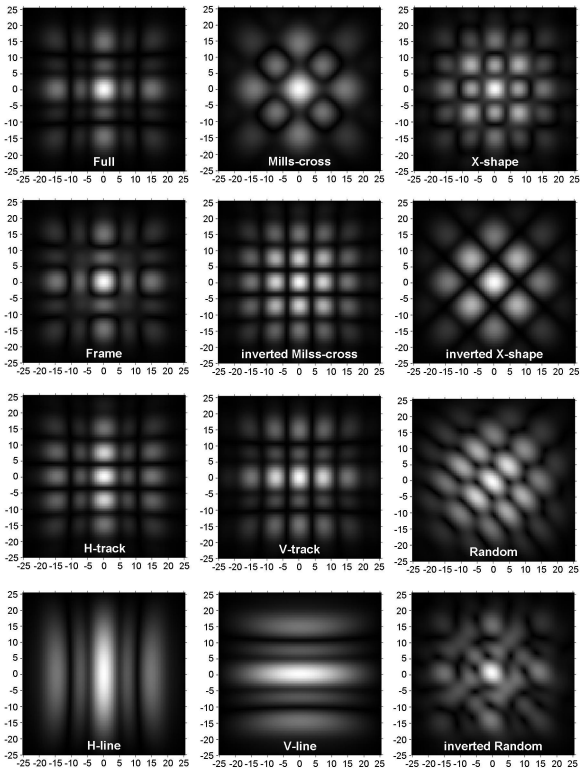

Figure 4. Acoustic field distributions $p(x,y,z)$ calculated for selected apertures of the 2-D transducer array in a 3 x 3 subarray, in water, for plane $x = y = -25$ mm ÷ 25 mm, at the distance of $z_o = 50$ mm from the surface of the array.

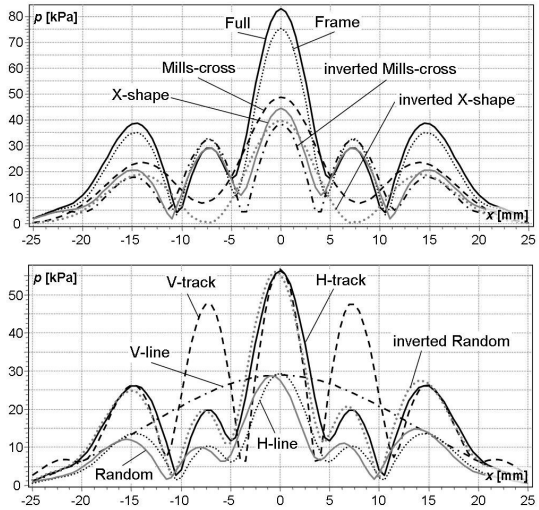

Figure 5. Comparison of the distribution of the values of the calculated acoustic pressure for the line of $y = 0$ images from Figure 4.

The calculated distribution of acoustic field generated in water by a single square 1.6 x 1.6 mm transducer (in the centre on the subarray) at the distance of 50 mm from the surface of the subarray is shown in Figure 6.

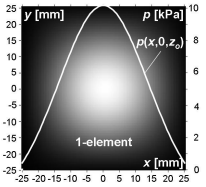

Figure 6. The calculated distribution of acoustic field generated by a single transducer (1.6 x 1.6 mm) in water, for plane $x = y = -25$ mm ÷ 25 mm, at the distance of $z_o = 50$ mm from the surface of the subarray.

Aperture distributions seem similar: *Full* ↔ *Frame*, *Mills-cross* ↔ *inverted X-shape* ↔ *inverted Random* ↔ *Random*, *X-shape* ↔ *inverted Millss-cross* ↔ *H-track* ↔ *V-track* (Figure 4). Due to symmetry of *H-track* and *V-track* as well as *H-line* and *V-line* apertures along the diagonal of the subarray, acoustic field distributions appropriately show the same property (compare Figure 2 and Figure 4). The highest value of acoustic pressure in the aperture axis can be observed for *Full* and *Frame* distribution, which are followed by *H-track* and *V-track* (Figure 5). This is associated with a large number of active transducers (Figure 2). *Full* and *Frame* distributions are characterised by highest directivity and lowest level of side lobes occurrence, both for *XOZ* and *YOZ* plane (Figure 5). High directivity and low level of side lobes is also observed for *H-track* distribution for *XOZ* plane and *V-track* distribution for *YOZ* plane (Figure 5). Although it allows achieving high acoustic pressure amplitude in the symmetry axis of the subarray, high directivity and low level of side lobes occurrence, activating a large number of the scanning subarray transducers can be unbeneficial due to the beforehand mentioned decrease in electrical impedance of the setup. Impedance of a single transducer of a multielement array, which has a 1.6 x 1.6 mm radiating surface and 2 MHz resonant frequency is several kΩ [13]. When activating 9 subarray transducers simultaneously, it causes decrease in electrical impedance of the setup to several hundred Ω. The best solution, in this case, is to select two different apertures for the scanning transmitting and receiving array that will guarantee high value of acoustic pressure, high directivity and low level of side lobes occurrence with acceptable decrease in electrical impedance of the transducer setup.

Sending-receiving aperture synthesis

In order to synthesize and visualise sending-receiving apertures of 2-D scanning subarrays in a transmission system for projection imaging, the authors of this study used formula (1) to calculate the product of acoustic field distribution $p_t(x,y,z)\cdot p_r(x,y,z)$ of the sending and receiving subarray. The product can be represented in acoustic pressure squared values (kPa^2) or in the values of voltage amplitude of the signal received by the receiving transducers $U_r(x,y,z)$, after linear rescaling using sensitivity values of the receiving system $S_r = U_r(0,0,z_{nf})/p_r(0,0,z_{nf})$ according the following formula:

$$U_r(x,y,z) = p_t(x,y,z)\cdot p_r(x,y,z)\cdot S_r, \tag{12}$$

where, in accordance to the definition of ultrasonic transducer sensitivity, z_{nf} indicates the length of its near field. The length of near field for a square ultrasonic transducer or an array can be determined using the following formula:

$$z_{nf} = \frac{a^2+b^2}{\pi\cdot\lambda}\left(1-\frac{a}{2b}\right) \approx 1.37\frac{a^2}{4\lambda}, \tag{13}$$

where a, b – the size of the square radiating aperture, λ – wave length. Sensitivity of a single receiving transducer can be determined using pressure piezoelectric constant of the piezoceramic material; g_{ik} [V/(m·Pa)]:

$$g_{ik} = \frac{U}{g\cdot P}\cdot \tag{14}$$

If a piezoceramic plate is affected by acoustic pressure changing in time $p_r(t)$, the plate's thickness alters because of its elasticity (squeezing, stretching), and the electric charges inducing in the plate result in a difference in potentials on the plate's covers. The biggest changes of thickness $g_r(t)$ an consequently voltage $u_r(t)$ are achieved, when the frequency of pressure changes is equal to resonant frequency of the plate.

Figure 7 shows the calculated product of acoustic field distributions in water for a pair of single square 1.6 x 1.6 mm transducers located in parallel and facing one another, in the centre of the sending and receiving subarray of 3 x 3 elements, at the distance of 50 mm from one another. Figure 8 shows products of acoustic field distributions calculated as before for suitable combinations of sending-receiving apertures (see Figure 2).

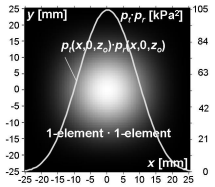

Figure 7. The calculated product of acoustic field distribution in water for a pair of single transducers of the sending and receiving subarray.

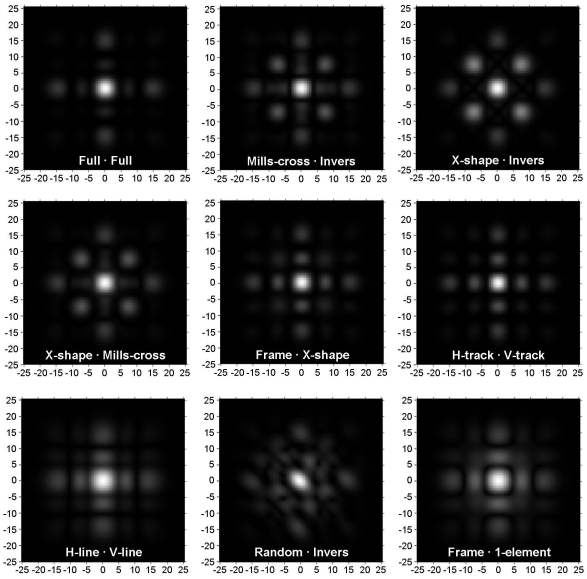

Figure 8. The calculated products of acoustic field distributions in water for suitable combinations of sending-receiving apertures.

Figure 9 compares the values of the products of acoustic pressure distributions of sending-receiving apertures for the line of $y = 0$ images from Figure 8.

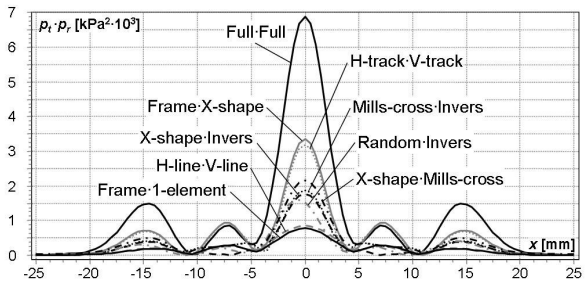

Figure 9. Comparison of the values of the products of acoustic pressure distributions of sending-receiving apertures for the line of $y = 0$ images from Figure 8.

All the calculated distribution products for suitable combinations of sending-receiving apertures (Figure 8) show significant ultrasonic wave beam narrowing and increase of the amplitude of the main lobe (Figure 9) in comparison to the distribution for 1-element combination (Figure 7). There is significant similarity between distribution products for the following aperture combinations: *Full·Full* ↔ *Frame·X-shape* ↔ *H-track·V-track*, *Mills-cross·Invers* ↔ *X-shape·Invers* ↔ *X-shape·Mills-cross*, *H-line·V-line* ↔ *Frame·1-element* (Figure 8). Distribution product for *Random·Invers* combination shows ellipsoidal deformation of the main lobe (the principal axis of the ellipsis is located on the diagonal of the image). The highest amplitude value for aperture axis is observed for *Full·Full* distribution product, followed by *Frame·X-shape* and *H-track·V-track*. The lowest value can be observed for *H-line·V-line* and *Frame·1-element* distribution products. This amplitude rises linearly with the increase of the product of activated sending transducers N_t and receiving transducers N_r and changes slightly depending on their mutual position (Figure 10).

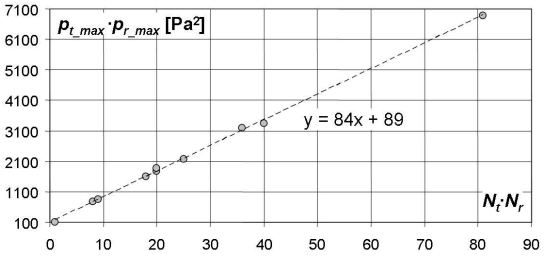

Figure 10. The dependence of the amplitude of distribution product for combinations of sending-receiving apertures from Figure 7 and Figure 8 determined at the central point (maximum level of the main lobe) on the product of active sending and receiving transducers.

The beam divergence angle (main lobe) of the distribution product of acoustic pressure for sending-receiving apertures from Figure 7 and Figure 8 demonstrates power law dependence on the product of active sending and receiving transducers and changes slightly depending on their mutual position (Figure 11). Above $N_t \cdot N_r = 20$, the beam divergence angle is approximately constant and equals about 4°. The difference in the maximum levels of the main lobe and side lobes changes horizontally in the scope of about 9 ÷ 13 dB in the range of $N_t \cdot N_r = 8 \div 81$ (Figure 12); for 1-element setup the difference is about 31 dB. Value dispersion probably depends on mutual position of sending and receiving transducers and the orientation of side lobe maximums (the relation presented in Figure 12 was determined for values of distribution along the x axis but as visible in Figure 8, some distributions have side lobe maximums along the y axis or along diagonals).

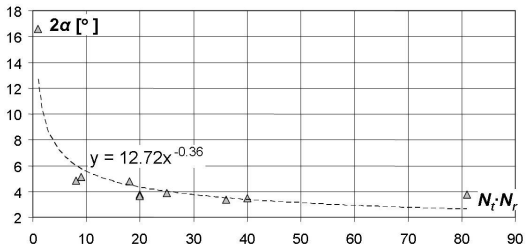

Figure 11. The dependence of the beam divergence angle of distribution products for combinations of sending-receiving apertures from Figure 7 and Figure 8 horizontally ($y = 0$, $x = -25 \div 25$ mm) on the product of active sending and receiving transducers.

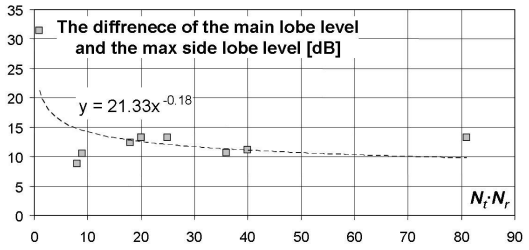

Figure 12. The dependence the difference in maximum levels of the main lobe and side lobes of distribution product for combinations of sending-receiving apertures from Figure 7 and Figure 8 horizontally ($y = 0$, $x = -25 \div 25$ mm) on the product of active sending and receiving transducers.

Measuring system and examined arrays

Automatic measurements of the acoustic field distribution for sample apertures of 2-D ultrasonic transducer arrays were made at the purpose-built measurement setup (Figure 13) [12,13].

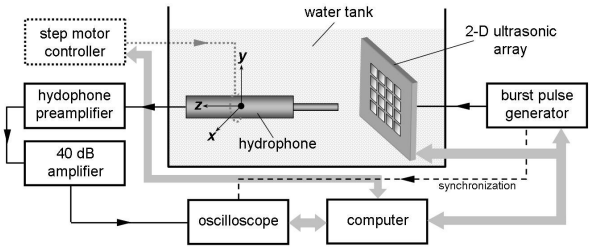

Figure 13. A block scheme of the setup for automatic measurements of the acoustic field distribution for ultrasonic transducers.

The examined array was fixed using a special stand in the tank with degassed distilled water, and there was a hydrophone HPM05/2 Precision Acoustics with diameter of 0.5 mm and sensitivity 939 mV/MPa at 2 MHz mounted on the travelling mechanism arms *XYZ*. A special electronic circuit board and software, which also enabled setting of pulse generator parameters using the GPIB interface were used for the control of electronic keys for switching the array elements using the RS232 serial port. Array transducers were activated using burst type pulses at repeat frequency $f_p = 1$ kHz, filled with a sinusoidal signal at $f \approx 2$ MHz and length of 10 cycles. The pulse amplitude was approximately 20 V_{pp}. The acoustic field generated by array elementary transducers was measured in water at the plane parallel to the array plane (perpendicular to the propagation direction).

Three kinds of 2-D arrays of piezoceramic transducers with surface dimensions of 1.6 x 1.6 mm each, in the layout of 3 x

3 and 4 x 4 elements, distributed evenly with spacing of 0.9 mm (distance between transducer centers d = 2.5 mm), operating with frequency $f \approx 2$ MHz (Figure 14).

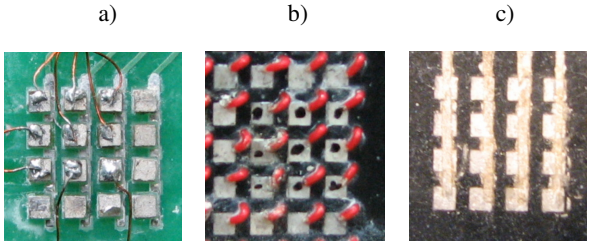

Figure 14. View of fragments of surface of examined 2-D arrays of piezoceramic transducers: a) *A1*, b) *A2*, c) *A3*.

A1 array transducers made of Pz37 Ferroperm piezoceramics were soldered on the side of ground connected electrodes to square conductive fields etched on the PCB board using hot air and positioned using the mask made of engraving laminate with laser precision-cut holes matched to dimensions of transducers (Figure 14a). After removing the laminate thin wire electrodes were soldered to radiating surfaces. Each *A1* array transducer can be activated independently. *A2* array transducers made of SONOX P2 CeramTec piezoceramics were glued on the side of ground connected electrodes to square paths etched on the PCB board using conductive glue and positioned using the mask made of engraving laminate (Figure 14b) [22]. The engraving laminate was glued to the surface of the PCB board. Insulated wire electrodes were connected to the radiating surface of transducers by means of springy contact (Figure 14b). Each *A2* array transducer can be activated independently. *A3* array transducers made of Pz37 Ferroperm piezoceramics were glued on the back side to square paths etched on the PCB board using conductive glue and positioned using the mask made of engraving laminate (Figure 14c). The engraving laminate was glued to the surface of the PCB board. Connections in columns were made on the radiating surface of transducers and laminate by means of paths made from conductive substance (Figure 14c). The *A3* array was used in both active [12] and passive [13] system using special sets of electronic keys, which enabled activation of individual transducers using schemes shown on Figure 15. In the active system, when activating one array element, the whole column (interchangeably with a row) [12] is activated in the appropriate way, and in the passive system, the whole array is activated upon activating one of its elements [13]. Such design of the array together with electronic switching elements allows to minimize electrode leads and maximize directivity [12,13].

Surfaces of array fragments, which were to be immersed in water were sprinkled with a transparent acrylate coating of good insulation properties, which additionally served as a layer for matching ultrasonic transducers impedance to the impedance of the load medium.

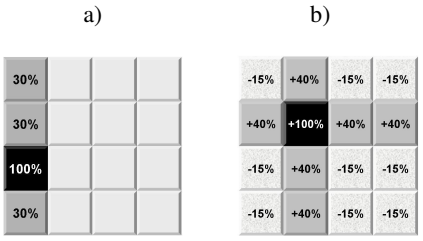

Figure 15. Distribution of voltages at *A3* array transducers when activating one element in the system: a) active – single columns, or interchangeably rows are activated [12], b) passive – the whole array is activated [13].

Results of measurements

Figure 16 shows measurements of amplitude (peak-to-peak) of the burst type pulse that activates *A1* and *A2* array transducers depending on the number of activated transducers. Number 0 means that only leads that feed the signal were connected to the generator. Trend lines are also drawn on the chart.

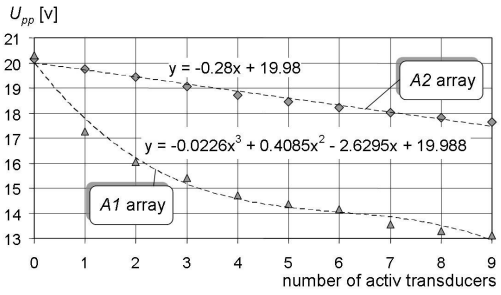

Figure 16. Amplitude of the burst type pulse voltage that activates *A1* and *A2* array transducers depending on the number of activated transducers.

Figure 17 shows the results of measurements of the acoustic field distribution at the layout of 3 x 3 *A1* array transducers measured in water using the needle hydrophone (0.5 mm diameter) for selected apertures, 50 mm from the array surface, at the area of 50 x 50 mm that is perpendicular to the array surface, with step of 0.5 mm.

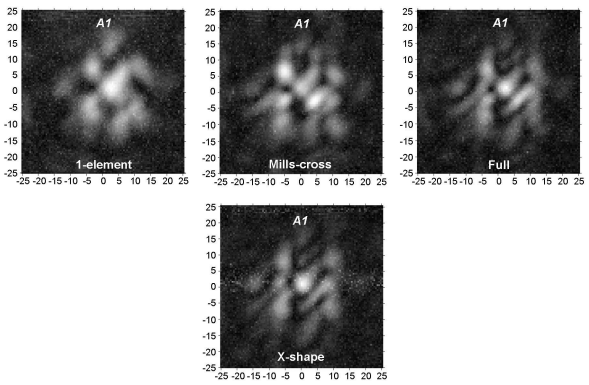

Figure 17. Acoustic field distribution at the layout of 3 x 3 *A1* array transducers measured in water for selected apertures.

These distributions (Figure 17) shall reveal similarity to relevant distributions from Figure 4 and Figure 6, however, distinct differences are visible that were caused mainly by load of the radiating surface of transducers as a result of soldering the electrodes (Figure 14a) [28]. The acoustic field distribution is also affected by the method of soldering of the back surface of array transducers (ground side).

Figure 18 shows the results of measurements of the acoustic field distribution at the layout of 3 x 3 *A2* array transducers [22] measured in water using the needle hydrophone (0.5 mm diameter) for selected apertures, 50 mm from the array surface, at the area of 50 x 50 mm that is perpendicular to the array surface, with step of 0.5 mm. These distributions (Figure 18) shall reveal similarity to relevant distributions from Figure 4 and Figure 6, however, distinct differences are visible that were caused mainly by scattering effect of electrodes with a large diameter comparing to the wavelength, located close to the surface of transducers (Figure 14b). The acoustic

field distribution is also affected by a non-uniform method of gluing of the back surface of array transducers (ground side).

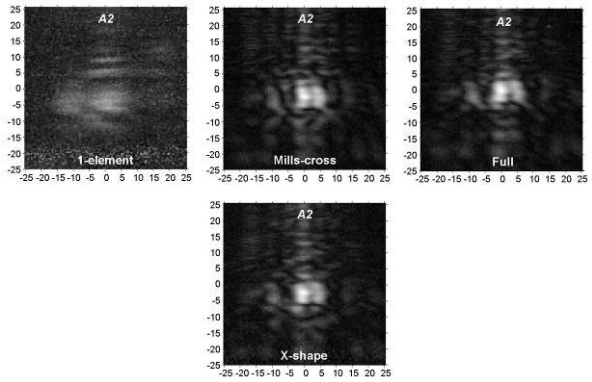

Figure 18. Acoustic field distribution at the layout of 3 x 3 *A2* array transducers measured in water for selected apertures.

The *A3* active array [12] was measured in the layout of 4 x 4 transducers in water, placed 50 mm from the array surface in the area of 40 x 40 mm that was parallel to the array surface, with the step of 0.5 mm, using the measuring needle hydrophone having the diameter of 0.5 mm. The hydrophone was placed in a way shown in Figure 19a in relation to the array surface. The *A3* passive array [13] was measured in the layout of 4 x 4 transducers in water, placed 25 mm from the array surface in the area of 20 x 20 mm that was parallel to the array surface, with the step of 0.5 mm using the ultrasonic measuring probe having the diameter of 5 mm [13]. The probe was placed in a way shown in Figure 19b in relation to the array surface. Probe was used instead of the hydrophone in order to smooth the measured acoustic field (close to near field) and to avoid its disturbances [13].

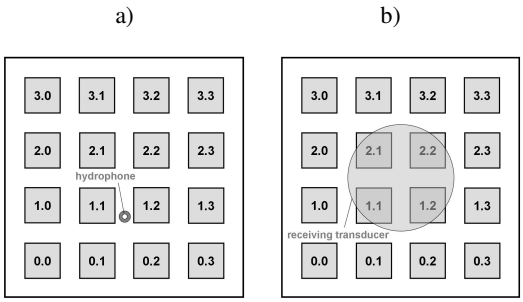

Figure 19. Numbering of *A3* array transducers in the layout of 4 x 4 and placing of: a) hydrophone when measuring the active array, b) receiving probe when measuring the passive array.

Figure 20 shows the results of calculations in comparison with measurements of the acoustic field distribution at the layout of 4 x 4 transducers of the *A3* active array [12] in the column configuration, measured in water at successive activation of transducers 2.0, 3.0 and 3.1 (Figure 14c, 15a, 19a). Piezoceramic transducers of the *A3* active array were carefully selected from a large batch by reason of the smallest possible scatter of the resonance frequency and electric impedance [12]. Additionally, the method of applying glue on the PCB board paths for gluing transducers was optimized for repeatability (Figure 14c); thin paths of conductive glue on the radiating side don't load transducers surfaces significantly. This makes the calculated and measured acoustic field distributions similar to one another (Figure 20) [12]. Small differences result mostly from possible inaccuracies of spacing of transducer in relation to one another (small rotation, displacements and inclinations on an irregular layer of glue) and inaccuracies of placement of the hydrophone in relation to the array.

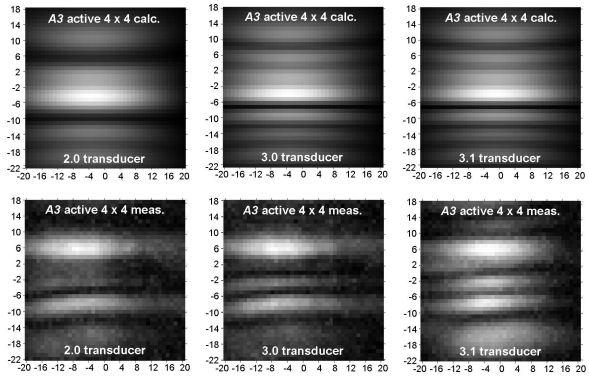

Figure 20. Comparison of results of calculations and measurements of the acoustic field distribution at the layout of 4 x 4 transducers of the *A3* active array in the column configuration.

Figure 21 shows the results of calculations in comparison with measurements of the acoustic field distribution at the layout of 4 x 4 transducers of the *A3* passive array [13] measured in water at successive activation of transducers 2.0, 3.0 and 3.1 (Figure 14c, 15b, 19b). All measured distributions are shown in a logarithmic scale [13] in order to depict minute differences in the acoustic pressure.

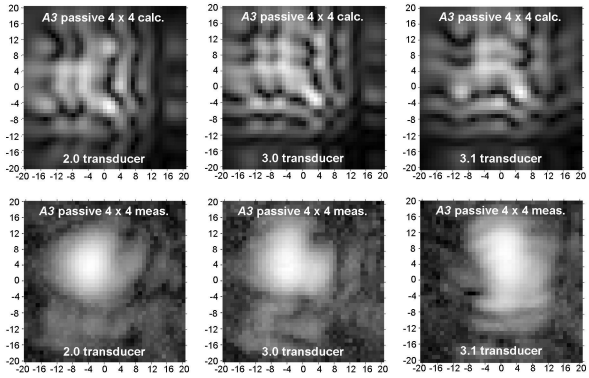

Figure 21. Comparison of results of calculations and measurements of the acoustic field distribution at the layout of 4 x 4 transducers of the *A3* passive array.

Calculated and measured acoustic field distributions show very good conformity (Figure 21) [13] for the same reasons as with the active array. Due to the use of the receiving probe with diameter of 5 mm [13] as a detector for measurements, the measured distributions are smoothed (Figure 21), but free of disturbances caused by the hydrophone needle, the diameter of which is comparable to the wavelength.

Figure 22 shows products of measured acoustic field distributions in the transmitting-receiving setup for selected combinations of the *A1* array apertures.

Figure 23 shows products of measured acoustic field distributions in the transmitting-receiving setup for selected combinations of the *A2* array apertures.

Due to the good conformity of calculations and measurements for the active and passive *A3* array, the sample synthesis of the transmitting-receiving aperture was done using simulated acoustic field distributions.

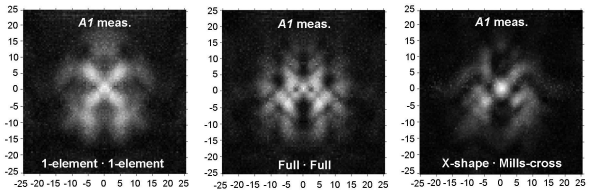

Figure 22. Products of measured acoustic field distributions in the transmitting-receiving setup for selected combinations of the *A1* array apertures.

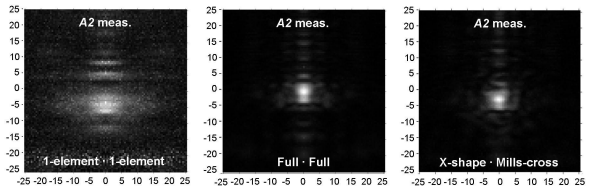

Figure 23. Products of measured acoustic field distributions in the transmitting-receiving setup for selected combinations of the *A2* array apertures.

Figure 24 shows the calculated acoustic field distribution in water generated by the *A3* active array in the layout of 4 x 4 transducers, for the column configuration (activation of no. 2.1 transducer in the transmitting array) and row configuration (activation of no. 2.2 transducer in the receiving array) and the product of these distributions in the transmitting-receiving set. Calculations were made for the distance of 50 mm from the array surface, at the area of 50 x 50 mm that is perpendicular to the array surface, with step of 0.5 mm.

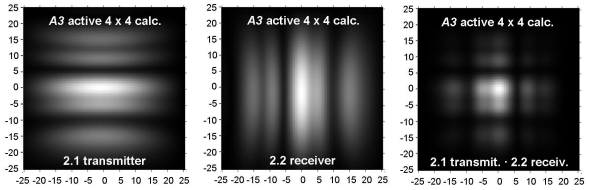

Figure 24. Calculated acoustic field distributions in water generated by the *A3* active array in the layout of 4 x 4 transducers for both column and row configurations and the product of these distributions in the transmitting-receiving set.

Figure 25 shows the calculated acoustic field distribution in water generated by the *A3* passive array in the layout of 4 x 4 transducers (activation of the no. 2.1 transducer in the transmitting array and no. 2.2 transducer in the receiving array) and the product of these distributions in the transmitting-receiving set. Calculations were made for the distance of 50 mm from the array surface, at the area of 50 x 50 mm that is perpendicular to the array surface, with step of 0.5 mm.

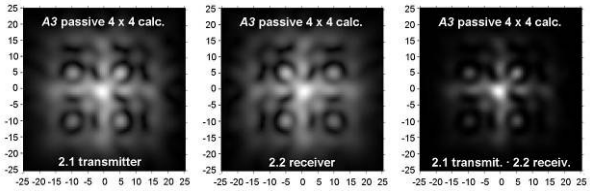

Figure 25. Calculated acoustic field distributions in water generated by the *A3* passive array in the layout of 4 x 4 transducers and the product of these distributions in the transmitting-receiving set.

CONCLUSIONS

The developed method for calculations of the acoustic field distribution at flat 2-D ultrasonic arrays made of square piezoceramic transducers is well suited for modelling the transmitting-receiving aperture of scanning subarrays systems in order to optimize the shape of the wave beam, increase of its intensity, and shaping the directivity characteristics in the method of projection imaging.

Due to the decrease of impedance that was proportional to the number of activated subarray transducers, matching to the voltage output of the burst type pulse generator and keeping a large area in the projection scanning plane it is advisable to use scanning subarrays that have a small number of transducers. Due to the symmetry of the system, the subarrays shall consist of an odd number of elements placed symmetrically in the square area. With a small scanning subarray (9 transducers), the decrease of voltage at the generator lessens, but does not important remove the gain in the field intensity that results from activation of a large number of transducers. In case of small subarrays the amplitude of the product of acoustic pressure distributions for the transmitting and receiving subarray aperture increases linearly with the increase of the product of active transmitting and receiving transducers and changes slightly depending on their configuration. The product of *Full·Full* distributions, then *Frame·X-shape* and *H-track·V-track* shows the highest amplitude value in the apertures axis.

Using appropriate combinations of apertures of the transmitting and receiving array allows to increasing the directivity of the ultrasonic wave beam and ensures its apodization in the transmission system. With a small scanning subarray (9 transducers) the angle of divergence of the main lobe of the product of acoustic pressure distributions for the transmitting and receiving aperture changes slightly with the increase of number of the product of transmitting and receiving aperture transducers, if this product number is more than 20. Decrease in the level of grating side lobes by about 9 ÷ 13 dB in relation to the main lobe can be obtained for many different combinations of the transmitting and receiving array apertures.

With small scanning subarray (9 transducers) the choice of the transmitting-receiving aperture combination depends mostly on the maximum amplitude criterion, as well as symmetry and uniformity of the power of acoustic pressure level distributions.

Both placing and connections of elementary piezoceramic transducers greatly affects the uniformity and distribution of the acoustic field. Best results were obtained due to minimization of the number of connections in the active and passive *A3* array system [12,13] and due to use of glued connections using the conductive glue. Therefore, a pair of *A3* active arrays (transmitting and receiving one) can be successfully used for projection imaging, where one array works in the column configuration, and another one in the row configuration; it is also possible to use *A3* arrays in the passive system for this purpose.

ACKNOWLEDGMENTS

This research was carried out as part of grant no. N N515 410634 funded by MNiSW (Ministry of Science and Higher Education of Poland) in the years 2008 – 2011.

REFERENCES

1 G.R.Lockwood, F.S.Foster, "Optimizing the Radiation Pattern of Sparse Periodic Two-Dimensional Arrays" *IEEE Transactions on Ultrasonics, Ferroelectrics, and Frequency Control*, **43**(1), 15–19 (1996).

2 K.E.Thomenius, "Evolution of ultrasound beamformers" *1996 IEEE Ultrasonics Symposium Proceedings*, 1615–1622 (1996).

3 D.G.Wildes, R.Y.Chiao, Ch.M.W.Daft, K.W.Rigby, L.S.Smith, K.E.Thomenius, "Elevation performance of 1.25D and 1.5D Transducer Arrays" *IEEE Transactions on Ultrasonics, Ferroelectrics, and Frequency Control*, **44**(5), 1027–1037. (1997).

4 J.T.Yen, S.W.Smith, "Real-Time Rectilinear 3-D Ultrasound Using Receive Mode Multiplexing" *IEEE Transactions on Ultrasonics, Ferroelectrics, and Frequency Control*, **51**(2), 216–226 (2004).

5 J.A.Johnson, M.Karaman, B.T.Khuri-Yakub, "Coherent-Array Imaging Using Phased Subarrays. Part I: Basic Principles" *IEEE Transactions on Ultrasonics, Ferroelectrics, and Frequency Control*, **52**(1), 37–50 (2005).

6 B.W.Drinkwater, P.D.Wilcox, "Ultrasonic arrays for non-destructive evaluation: A review" *NDT&E International*, **39**, 525–541 (2006).

7 J-J.Kim, T-K.Song, "Real-Time High-Resolution 3D Imaging Method Using 2D Phased Arrays Based on Sparse Synthetic Focusing Technique" *2006 IEEE Ultrasonics Symposium Proceedings*, 1995–1998 (2006).

8 I.O.Wygant, M.Karaman, Ö.Oralkan, B.T.Khuri-Yakub, "Beamforming and hardware design for a multichannel front-end integrated circuit for real-time 3D catheter-based ultrasonic imaging" *SPIE Medical Imaging*, **6147**, 61470A-1–8 (2006).

9 I.O.Wygant, H.Lee, A.Nikoozadeh, D.T.Yeh, Ö.Oralkan, M.Karaman, B.T.Khuri-Yakub, "An Integrated Circuit with Transmit Beamforming and Parallel Receive Channels for Real-Time Three-Dimensional Ultrasound Imaging" *2006 IEEE Ultrasonics Symposium Proceedings*, 2186–2189 (2006).

10 M.Karaman, I.O.Wygant, Ö.Oralkan, B.T.Khuri-Yakub, "Minimally Redundant 2-D Array Design for 3-D Medical Ultrasound Imaging" *IEEE Transactions on Medical Imaging*, **28**(7), 1051–1061 (2009).

11 K.J.Opieliński, T.Gudra, P.Pruchnicki, "The method of a medium internal structure imaging and the device for a medium internal structure imaging" *Patent Application to the Patent Office of the Republic of Poland,* P389014, Wroclaw University of Technology, (2009), in Polish.

12 K.J.Opieliński, T.Gudra, P.Pruchnicki, "A Digitally Controlled Model of an Active Ultrasonic Transducer Matrix for Projection Imaging of Biological Media" *Archives of Acoustics,* 3**5**(1), 75–90 (2010).

13 K.J.Opieliński, T.Gudra, P.Pruchnicki "Narrow Beam Ultrasonic Transducer Matrix Model Projection Imaging of Biological Media" *Archives of Acoustics,* 3**5**(1), 75–90 (2010).

14 R.Y.Chiao, L.J.Thomas, "Aperture formation on reduced-channel arrays using the transmit-receive apodization matrix" *1996 IEEE Ultrasonics Symposium Proceedings*, 1567–1571 (1996).

15 M.D.C.Eames, J.A.Hossack, "Fabrication and evaluation of fully-sampled, two-dimensional transducer array for "Sonic Window" imaging system" *Ultrasonics*, **48**, 376–383 (2008).

16 P.S.Green, L.F.Schaefer, E.D.Jones, J.R.Suarez, "A New High Performance Ultrasonic Camera" *Acoustical Holography*, **5**, 493–503 (1974).

17 H.Brettel, U.Roeder, C.Scherg, "Ultrasonic transmission camera for medical diagnosis" *Biomedizinische Technik*, **26**, 63 (1981).

18 B.Granz, R.Oppelt, "A Two Dimensional PVDF Transducer Matrix as a Receiver in an Ultrasonic Transmission Camera" *Acoustical Imaging*, **15**, 213–225 (1987).

19 H.Ermert, O.Keitmann, R.Oppelt, B.Granz, A.Pesavento, M.Vester, B.Tillig, V.Sander, "A New Concept For A Real-Time Ultrasound Transmission Camera" *IEEE Ultrasonics Symposium Proceedings*, San Juan, Puerto Rico 1611–1614 (2000).

20 K.J.Opielinski, T.Gudra, "Biological Structure Imaging by Means of Ultrasonic Projection" in *Acoustical Engineering* ed. R.Panuszka (Polish Acoustical Society, Krakow, Poland, 2004) pp. 97–106.

21 K.J.Opielinski, T.Gudra, "Computer recognition of biological objects' internal structure using ultrasonic projection" in *Computer recognition systems (Advances in Soft Computing)* ed. M.Kurzynski (Springer, Berlin, 2005) pp.645–652.

22 K.J.Opielinski, T.Gudra, "Multielement ultrasonic probes for projection imaging" *Physics Procedia*, **3**, 635–642, (2009).

23 K.J.Opielinski, T.Gudra, "Multi-parameter ultrasound transmission tomography of biological media" *Ultrasonics,* **44**, e295–e302 (2006).

24 T.Gudra, K.Opielinski, "The multi-element probes for ultrasound transmission tomography" *Journal de Physique IV*, **137**, 79–86 (2006).

25 K.J.Opielinski, T.Gudra, "Determining the acoustic field distribution of ultrasonic multi-element probes" *Archives of Acoustics*, **31**(4), 391–396 (2006).

26 T.Gudra, K.J.Opielinski, "The ultrasonic probe for the investigating of internal object structure by ultrasound transmission tomography" *Ultrasonics,* **44**, e679–e683 (2006).

27 R.T.Hoctor, S.A.Kassam, "The Unifying Role of the Coarray in Aperture Synthesis for Coherent and Incoherent Imaging" *Proceedings of the IEEE*, **78**(4), 735–752 (1990).

28 E.K.Sittig, "Effects of Bonding and Electrode Layers on the Transmission Parameters of Piezoelectric Transducers Used in Ultrasonic Digital Delay Lines" *IEEE Transactions on Sonics and Ultrasonics*, **16**(1), 2–10 (1969).